Development of a Soil EC_a Inversion Algorithm for Topsoil Depth Characterization

Eko Leksono[1], Viacheslav Adamchuk[1], Wenjun Ji[2], Maxime Leclerc[1]

[1]Bioresource Engineering Dept., McGill University, Ste-Anne-de-Bellevue, QC, Canada
[2]Soil and Environment Dept., Swedish University of Agricultural Sciences, Skara, Sweden

A paper from the Proceedings of the
14th International Conference on Precision Agriculture
June 24 – June 27, 2018
Montreal, Quebec, Canada

Abstract. *Electromagnetic induction (EMI) proximal soil sensor systems can deliver rapid information about soil. One such example is the DUALEM-21S (Dualem, Inc. Milton, Ontario, Canada). EMI sensors measure soil apparent electrical conductivity (EC_a) corresponding to different depth of investigation depending on the instrument configuration. The interpretation of the EC_a measurements is not straightforward and it is often site-specific. Inversion is required to explore specific depths. This inversion process is an “ill-posed” problem which might lead to non-existing, or non-unique solutions. Commonly, a complicated regularization method is chosen to tackle this problem. In this paper, a simple exhaustive “brute-force” method was developed to characterize soil layering depths and their corresponding EC_a values. A two-layer soil EC_a model was used to depict the depth of the topsoil layer and its corresponding EC_a value. The two-layer model represents a shallow (topsoil) and deeper subsoil depths. From the high density DUALEM-21S input data, the “brute-force” algorithm was successfully converged to the minimum mean squared error (MSE) for each depth increment. The software’s GUI was intuitive and provided an up to date progress of the calculations. This algorithm has been tested successfully to determine the topsoil and subsoil EC_a values together with muck soil layer depth on the 25-ha field near Naperville, Quebec, Canada.*

Keywords. electromagnetic induction, soil EC_a, inversion, topsoil depth.

Introduction

One step in implementing precision agriculture (PA) practices is data collection, which utilizes various sensors to recognize the characteristics of numerous on-farm components (Srinivasan, 2006). Proximal soil sensors, such as electromagnetic induction (EMI) sensors, can deliver spatial and temporal information about soil. EMI sensors measure soil apparent electrical conductivity (EC_a) and they have become a common way to rapidly characterize soil heterogeneity. DUALEM-21S (Dualem, Inc., Milton, Ontario, Canada) is a popular example of an EMI sensor used in precision agriculture. DUALEM-21S is a sensor with a dipole configuration (the distance of the receivers to transmitter coil are more than ten times the diameter of the transmitter loop) and fixed working frequency of 9 kHz (Daniels et al., 2008). It has one vertical transmitter (Tx) coil with 2 sets of receivers (Rx) coils spaced 1 and 2 m for horizontal coplanar orientation (HCP) and 1.1 and 2.1 m for perpendicular coil orientation (PRP).

The interpretation of EC_a readings was not straightforward and often it was site-specific (Bronson et al., 2005; Pedrera-Parrilla et al., 2016), as conduction in soil can be affected by various factors, such as soil water content (Brevik et al., 2006), clay content (Sun et al., 2011), soil temperature (Padhi and Misra, 2011), mineralogy (McNeill, 1980a) and salinity (Corwin and Lesch, 2003). Therefore, cross validation with standard laboratory measurements together with expert interpretation were essential to provide reliable information (Doolittle and Brevik, 2014). Despite its interpretation complexity, EC_a measurements from EMI sensors also provide information about change of EC_a magnitude with depth. The process to obtain this information is called inversion. Inversion is an ill-posed problem which commonly is solved by regularization, followed by stabilization through selecting the best possible solution (Zhdanov, 2015). Generally, there are two versions of EMI inversion, the finite element method and the fixed slice cumulative depth response approach.

The finite element inversion approach has been used extensively with various EMI sensors, such as EM34 (Fernando A. Monteiro Santos, 2004), EM38-EM31 (Triantafilis and Santos, 2010), EM38-EM34 (Triantafilis and Santos, 2009), and DUALEM 421 (F. A. Monteiro Santos et al., 2010; Triantafilis et al., 2011; Huang et al., 2016) with acceptable results. In general, the finite element inversion will generate a stronger correlation between inverted EC_a results and measured soil properties, if using joint data from various EMI sensors (Triantafilis et al., 2013; Triantafilis and Monteiro Santos, 2013). On the other hand, the fixed slice cumulative depth response approach has been used for archaeological mapping (Timothy Saey et al., 2008; Timothy Saey et al., 2012b; De Smedt et al., 2013), detecting the depth of clay layers (T. Saey et al., 2009) and identifying ploughing depths (Timothy Saey et al., 2012a). The method started with the determination of several fixed soil depth slices and is then followed by EC_a forward calculation using the EMI cumulative response and modelled EC_a at a specified depth slice. Further, the calculated EC_a was compared with the measured EC_a to assess the misfit value. The initial EC_a model was further iterated with a fixed depth step (i.e., every 1 cm (Sudduth et al., 2013)) until it reached a specified iteration number. Another option is to use the Levenberg-Marquardt minimization algorithm to reach the convergence solution. However, often, this minimization algorithm did not converge into an acceptable solution (Timothy Saey et al., 2012b).

In this research, an exhaustive “brute-force” method was developed to characterize soil layering depths and their corresponding EC_a values. DUALEM-21S has four measurement modes; hence, it can be used to generate up to four unknowns characterizing the soil profile. Thus, a two layer soil EC_a model was sufficient to depict the depth of the topsoil layer and its corresponding EC_a value. The two-layer model represents a shallow (topsoil) and deeper subsoil depths, which was expected to be sufficient to determine depth of muck soil over clay subsoil in a Quebec vegetable production farm.

Materials and Methods

1. Response Function

EMI sensors measure soil EC_a under the assumption of linearity between measured EC_a and the true homogeneous halfspace conductivity. The linear relationship only holds at the low induction number (< 100 mS m^{-1}) (McNeill, 1980b). The induction number is the ratio of inter coil spacing to skin depth. The depth where the primary field is attenuated to 1/e (36.8%) is called skin depth. Within this range, soil EC_a can be described as:

$$EC_a = \frac{4}{\omega\mu_0 s^2} {H_s}/{H_p} \quad (S\, m^{-1}) \tag{1}$$

where: ω = 2πf (s^{-1}), f = frequency (Hz), μ_0 = permeability of free space (1.25663706 x 10^{-6} m kg s^{-2} A^{-2}), s = primary to secondary coil (inter coil) separation (m), H_s = secondary electromagnetic field at the receiver coil and H_p = primary electromagnetic field at receiver coil (A m^{-1}).

Soil is not uniform and hence, there are various permeability levels (Patitz et al., 1995). Therefore, EC_a interpretation needs special training and often requires other sensors to validate the EC_a measurement. Under the low induction number (LIN) assumption, the relative (ϕ) and cumulative (R) depth response function for vertical (v), and perpendicular (p) coils are the following:

for vertical dipole orientation (HCP),

$$\varphi_v(z) = 4(z)(4z^2+1)^{-3/2} \tag{2}$$

$$R_v(z) = 1-(4z^2+1)^{-1/2} \tag{3}$$

while for perpendicular dipole orientation (PRP),

$$\varphi_p(z) = 2(4z^2+1)^{-3/2} \tag{4}$$

$$R_p(z) = 2z\,(4z^2+1)^{-1/2} \tag{5}$$

where z is normalized depth (soil depth divided by inter coil spacing). Following are the graphs of relative and cumulative depth response functions:

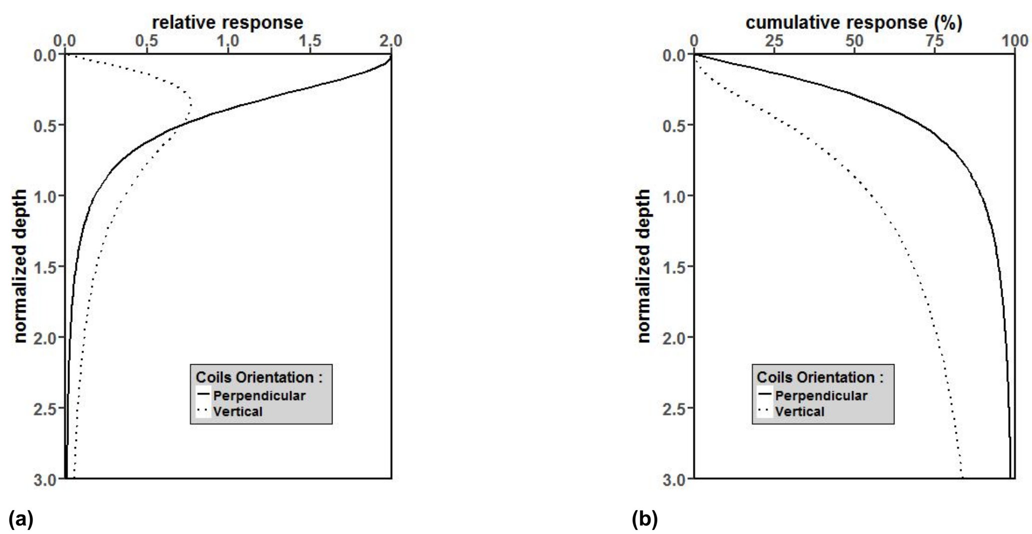

Fig. 1 DUALEM-21S Response Function: (a) Relative and (b) Cumulative Response Function

The response of the n-th soil layer to the cumulative EC_a (σ_a^c) can be described as:

$$\sigma_a^c = \sigma_1 R_{(z_1)} + \sum_{i=2}^{n-1} \sigma_i\left[R_{(z_i)} - R_{(z_{i-1})}\right] + \sigma_n\left[1-R_{(z_{n-1})}\right] \tag{6}$$

where σ_1 is a zero (air) conductivity since EMI sensor might be used at different height to particularly examine a specific depth of interest.

2. Brute-Force Algorithm

The fixed slice cumulative depth response approach was selected as a base method to invert the soil EC_a measurement. Matlab R2015b (MathWorks Inc. Natick, Massachusetts, USA) was used as a platform to develop the algorithm and its Graphical User Interface (GUI). The two-layer model was used to represent a shallow root zone (topsoil) and deeper subsoil. The soil depth increment was set to 5 cm with a maximum depth of 150 cm. The modification from the existing approach relies on replacing Levenberg-Marquardt minimization into an exhaustive “brute-force” algorithm. Furthermore, the calculated EC_a model was iterated based on the modelled soil EC_a value instead of incrementing the soil depth.

The modified algorithm can be described as follows: assume that at a specific location the algorithm needs to calculate the soil EC_a at the first 10 cm depth and below. The base setup matrices are:

$$\sigma_a^{cd} \times \mathrm{D} = \sigma_a^{calc} \tag{7}$$

where σ_a^{cd} is 4 x 2 matrix consisting of DUALEM-21S cumulative EC_a response at top (d) and deep (>d) soil depth, D is 2 x 1 matrix consisting of the modelled top (σ_d) and deep soil EC_a ($\sigma_{>d}$), σ_a^{calc} is 4 x 1 matrix consisting of calculated EC_a value for all DUALEM-21S coil orientations.

The inversion process was started by defining each DUALEM-21S measurement mode with its top (R_d) and deep ($R_{>d}$) soil cumulative depth response from (3) and (5) to form σ_a^{cd} matrix. Then, forward calculation was performed to estimate the calculated EC_a (σ_a^{calc} matrix) from the DUALEM-21S cumulative response function (σ_a^{cd} matrix) and the modelled EC_a value (D matrix). The calculated EC_a value was then subtracted with the measured EC_a to get the misfit value by using Root Mean Squared Error (RMSE) method. The maximum modelled EC_a value was set to 200 mS m^{-1} as this is the typical non-saline field (Staff, 2014), with resolution of 0.2 mS m^{-1}. Therefore, there are one million combinations of σ_d and $\sigma_{>d}$.

After all iterations, the cumulative depth response values of σ_a^{cd} matrix were changed at 10 cm depth increment then proceeded with similar processes. Since the topsoil has a maximum 150 cm depth, therefore, we have fifteen sets of σ_d and $\sigma_{>d}$. The appropriate depth combination solution would be the one that has the lowest RMSE value. The inversion flowchart can be seen in Fig. 2.

3. DUALEM-21S Mapping

DUALEM-21S mapping was performed at 25-ha field located at Napierville, Quebec, Canada (Fig. 3). The sampling rate was set at 1 Hz resulting in an approximate 5 m separation distance between records (mean of 10 consecutive measurements). The distance between transects was set to 10 m. Before starting the inversion, all EC_a data points were reduced to achieve equal spatial resolution between points using decimation method. Thus, 2828 DUALEM-21S data were used for the “brute-force” inversion from the initial 5655 data points. After the inversion was done, the resulting σ_d and $\sigma_{>d}$ was spatially interpolated using Ordinary Kriging option for Geostatistical Analyst in ArcMap 10.4.1 (ESRI, Redlands, California, USA).

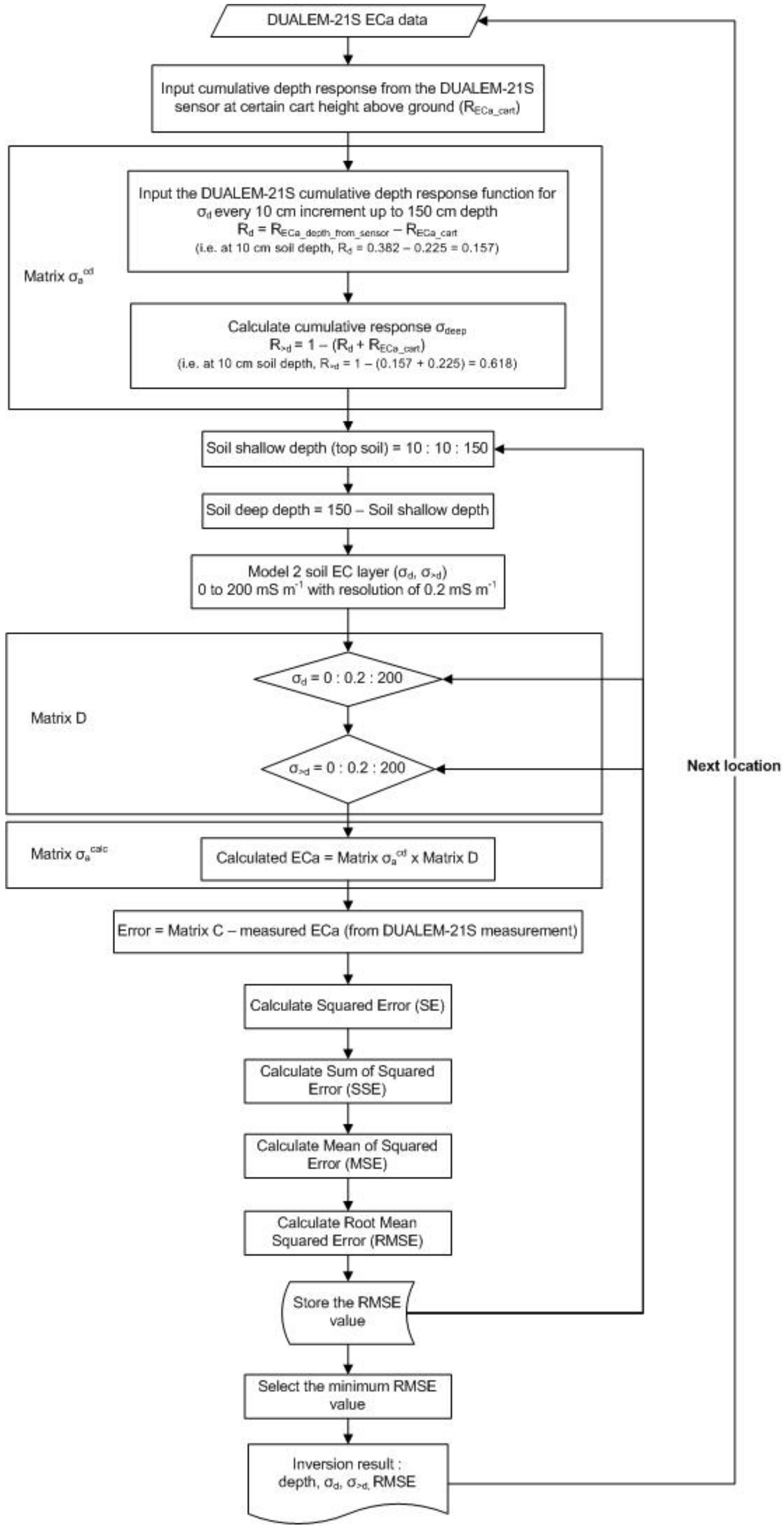

Fig. 2 DUALEM-21S Brute-Force EC_a Inversion Flow Chart

Fig. 3 DUALEM-21S Mapping Location

Results and DIscussions

Fig. 4 represents the GUI of the brute-force inversion software. There are two *.csv input files needed for the software to run: DUALEM-21S measurement data and cumulative depth response. User can monitor or cancel the inversion process anytime. A completion process screen will prompt the user if the inversion is finished. The inversion result was saved into the *.xlsx file format and stored in the same folder as the initial DUALEM-21S measurement data.

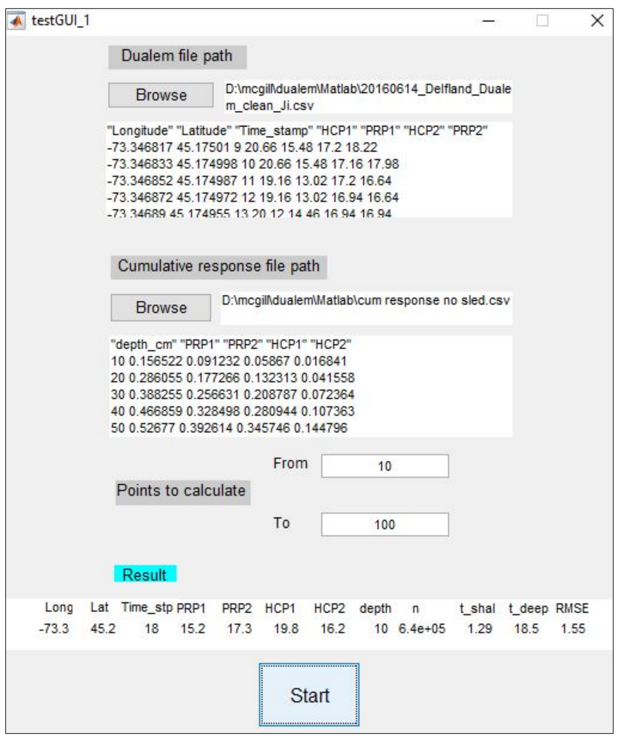

Fig. 4 The Brute-Force Inversion Software GUI

In one soil depth combination (i.e., topsoil depth d = 10 cm and deep soil depth d > 10 cm), the inversion process results in one million σ_d (shallow) and $\sigma_{>d}$ (deep) EC_a values with their corresponding RMSE (Fig. 5). Then the inversion software will select the minimum RMSE. After all depth combinations are inverted (Fig. 6), the algorithm selects the minimum RMSE from the successive depth increments; in this illustration, it was 10 cm which means that the depth of topsoil layer in this location was 10 cm. These processes were repeated for each location.

The example of brute-force inversion results along 110 m transect are shown in Fig. 7. This figure suggests that the depth of shallow EC_a layer was between 5 to 10 cm which positively correlate with shallot rooting depth. However, this result needs to be validated through laboratory soil sampling or direct soil EC measurements using EC probe. Furthermore, the shallow layer seems to have very low EC_a (< 5 mS m^{-1}). This may correspond to very dry and loose soil. Finally, as previously mentioned, the brute-force inversion does not create any smoothing between shallow and deep layers. Therefore, the inversion result may not represent the real soil EC gradient. Three-dimensional spatial interpolation might become alternative to achieve a smooth transition between shallow and deep EC_a layers.

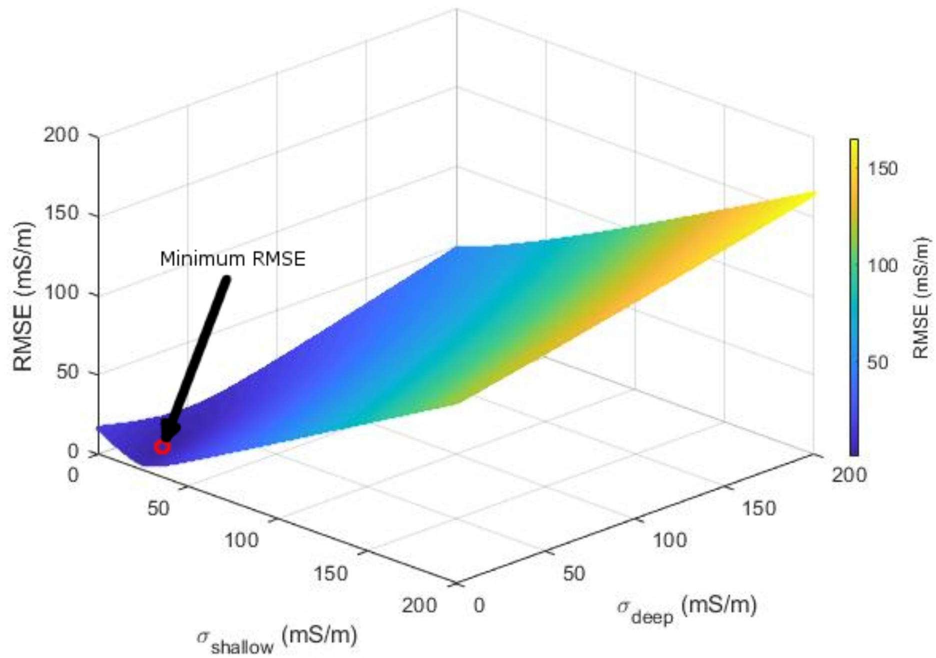

Fig. 5 Three-Dimensional Graph of σ_d (shallow), $\sigma_{>d}$ (deep) and their RMSE at d = 10 cm

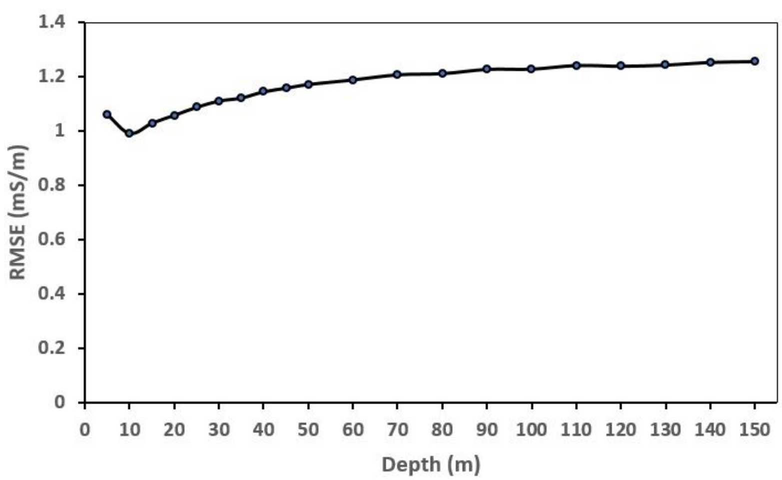

Fig. 6 Example of Brute-Force Inversion RMSE Value from 10 cm Depth Increments on One Selected Location

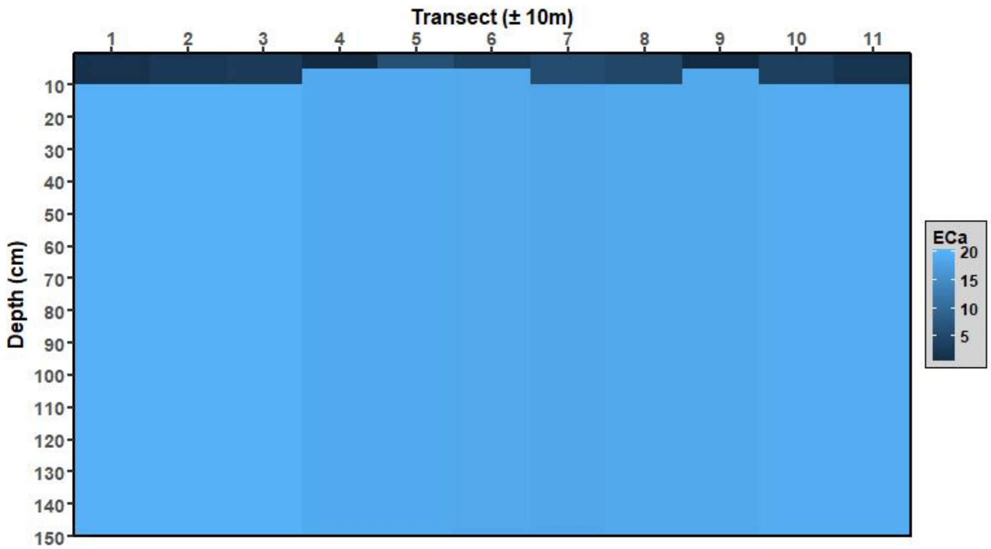

Fig. 7 Example of EC_a Shallow and Deep Along 11 Transect Points

The brute-force inversion result map for shallow and deep EC_a are shown in Fig. 8. High soil EC_a at shallow depths shown in the east to south-east area of the field (Fig. 8a) corresponds to wet conditions as we observed when surveying. In the deep EC_a map (Fig. 8b), high EC_a shown in the east to north-east side of the field corresponds to the drainage trench. Moreover, the nursery field located on the east side of the field was regularly sprayed with water which might contribute to higher soil EC_a values. Overall, the EC_a maps look realistic with smooth transitions.

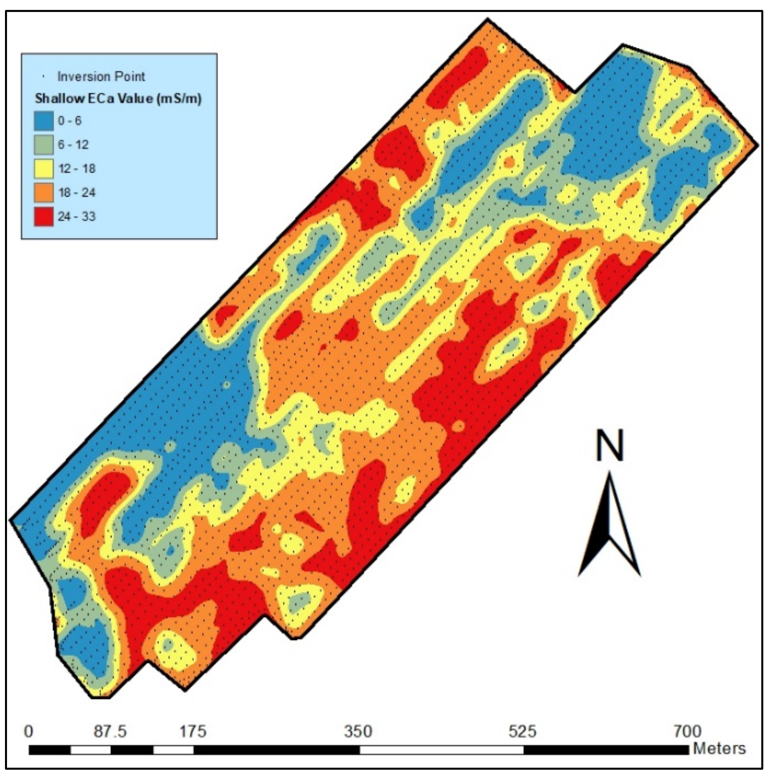

(a)

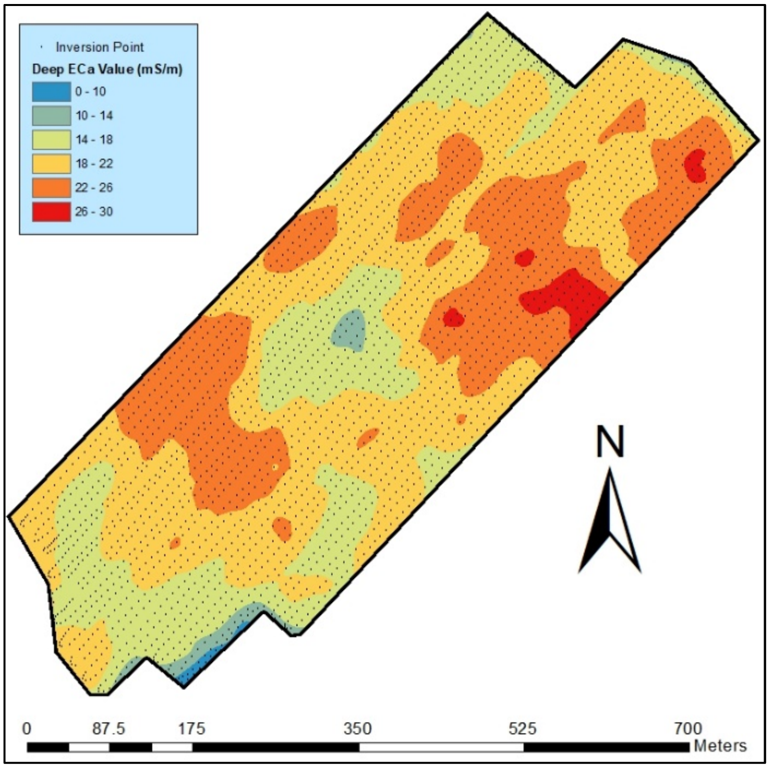

(b)

Fig. 8 Inversion Map: (a) Shallow EC$_a$, (b) Deep EC$_a$

Another brute-force inversion result is depth of topsoil (shallow) layer as shown in Fig. 9. From this map, the user can calculate the volume and the average depth of topsoil. The volume of the topsoil layer is 222,656.4 m^3 with an average depth of 88.9 cm. According to the farmer, the topsoil type is muck soil. Therefore, knowing the volume and georeferenced depth of the muck soil layer provide farmers with valuable information for adjusting their soil management practices.

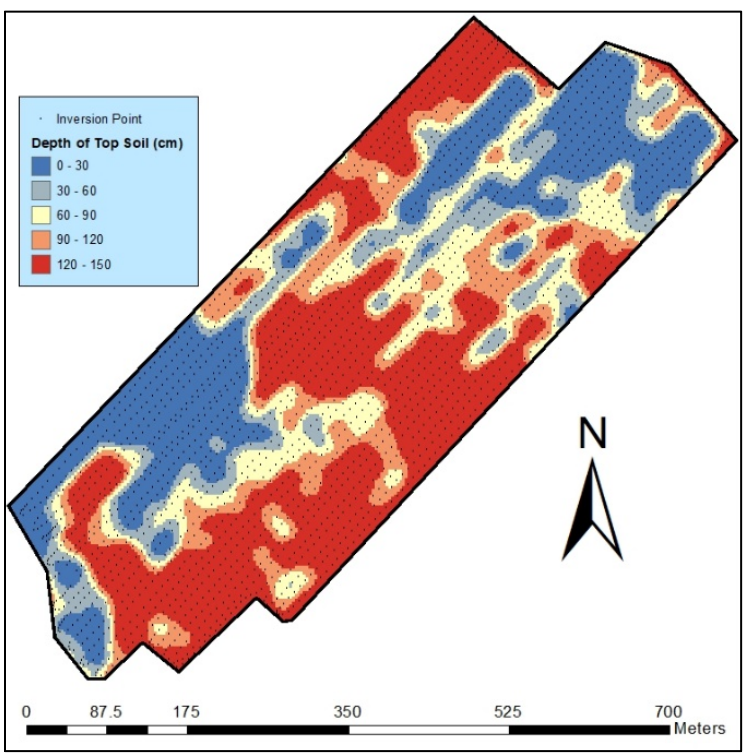

Fig. 9 Depth of Topsoil Layer

Conclusion

In this study a brute-force method was applied to develop a software for determining spatially variable two-layer model that could characterize change of EC_a with depth.

Acknowledgements

This research was supported in part by Indonesia Endowment Fund for Education (LPDP) and the National Science and Engineering Research of Canada (NSERC) Discovery Grant.

References

Brevik, E. C., Fenton, T. E., & Lazari, A. (2006). Soil electrical conductivity as a function of soil water content and implications for soil mapping. [journal article]. *Precision Agriculture, 7*(6), 393-404, doi:10.1007/s11119-006-9021-x.

Bronson, K. F., Booker, J. D., Officer, S. J., Lascano, R. J., Maas, S. J., Searcy, S. W., et al. (2005). Apparent Electrical Conductivity, Soil Properties and Spatial Covariance in the U.S. Southern High Plains. [journal article]. *Precision Agriculture, 6*(3), 297-311, doi:10.1007/s11119-005-1388-6.

Corwin, D. L., & Lesch, S. M. (2003). Application of Soil Electrical Conductivity to Precision Agriculture. *Agronomy Journal, 95*(3), 455-471, doi:10.2134/agronj2003.4550.

Daniels, J., Vendl, M., Reza Ehsani, M., & Allred, B. (2008). Electromagnetic Induction Methods. In *Handbook of Agricultural Geophysics* (pp. 109-128, Books in Soils, Plants, and the Environment): CRC Press.

De Smedt, P., Saey, T., Lehouck, A., Stichelbaut, B., Meerschman, E., Islam, M. M., et al. (2013). Exploring the potential of multi-receiver EMI survey for geoarchaeological prospection: A 90 ha dataset. *Geoderma, 199*, 30-36, doi:http://doi.org/10.1016/j.geoderma.2012.07.019.

Doolittle, J. A., & Brevik, E. C. (2014). The use of electromagnetic induction techniques in soils studies. *Geoderma, 223–225*, 33-45, doi:http://dx.doi.org/10.1016/j.geoderma.2014.01.027.

Huang, J., Scudiero, E., Choo, H., Corwin, D. L., & Triantafilis, J. (2016). Mapping soil moisture across an irrigated field using electromagnetic conductivity imaging. *Agricultural Water Management, 163*, 285-294, doi:http://doi.org/10.1016/j.agwat.2015.09.003.

McNeill, J. D. (1980a). Electrical Conductivity of Soils and Rocks. *Technical Note 5*. Ontario, Canada: Geonics Limited.

McNeill, J. D. (1980b). Electromagnetic Terrain Conductivity measurement at Low Induction Numbers. *Technical Note 6*. Ontario, Canada: Geonics Limited.

Padhi, J., & Misra, R. K. (2011). Sensitivity of EM38 in determining soil water distribution in an irrigated wheat field. *Soil and Tillage Research, 117*, 93-102, doi:http://doi.org/10.1016/j.still.2011.09.003.

Patitz, W. E., Brock, B. C., & Powell, E. G. (1995). Measurement of Dielectric and Magnetic Properties of Soil. (pp. 26). Albuquerque, New Mexico 87185 and Livermore, California 94550: Sandia National Laboratories.

Pedrera-Parrilla, A., Van De Vijver, E., Van Meirvenne, M., Espejo-Pérez, A. J., Giráldez, J. V., & Vanderlinden, K. (2016). Apparent electrical conductivity measurements in an olive orchard under wet and dry soil conditions: significance for clay and soil water content mapping. [journal article]. *Precision Agriculture, 17*(5), 531-545, doi:10.1007/s11119-016-9435-z.

Saey, T., De Smedt, P., Islam, M. M., Meerschman, E., Van De Vijver, E., Lehouck, A., et al. (2012a). Depth slicing of multi-receiver EMI measurements to enhance the delineation of contrasting subsoil features. *Geoderma, 189–190*, 514-521, doi:http://dx.doi.org/10.1016/j.geoderma.2012.06.010.

Saey, T., De Smedt, P., Meerschman, E., Islam, M. M., Meeuws, F., Van De Vijver, E., et al. (2012b). Electrical Conductivity Depth Modelling with a Multireceiver EMI Sensor for Prospecting Archaeological Features. *ARP Archaeological Prospection, 19*(1), 21-30.

Saey, T., Simpson, D., Vermeersch, H., Cockx, L., & Van Meirvenne, M. (2009). Comparing the EM38DD and DUALEM-21S Sensors for Depth-to-Clay Mapping. *Soil Science Society of America Journal, 73*(1), 7-12, doi:10.2136/sssaj2008.0079.

Saey, T., Simpson, D., Vitharana, U. W. A., Vermeersch, H., Vermang, J., & Van Meirvenne, M. (2008). Reconstructing the paleotopography beneath the loess cover with the aid of an electromagnetic induction sensor. *CATENA, 74*(1), 58-64, doi:http://doi.org/10.1016/j.catena.2008.03.007.

Santos, F. A. M. (2004). 1-D laterally constrained inversion of EM34 profiling data. *Journal of Applied Geophysics, 56*(2), 123-134, doi:http://dx.doi.org/10.1016/j.jappgeo.2004.04.005.

Santos, F. A. M., Triantafilis, J., Bruzgulis, K. E., & Roe, J. A. E. (2010). Inversion of Multiconfiguration Electromagnetic (DUALEM-421) Profiling Data Using a One-Dimensional Laterally Constrained Algorithm. *Vadose Zone Journal, 9*(1), 117-125, doi:10.2136/vzj2009.0088.

Srinivasan, A. (2006). *Handbook of Precision Agriculture*. New York: Food Products Press.

Staff, S. S. (2014). Soil Survey Investigations Report No. 51 Version 2. In R. Burt (Ed.), *Soil Survey Field and Laboratory Methods Manual* (pp. 265). Nebraska: Department of Agriculture, Natural Resources Conservation Service.

Sudduth, K. A., Myers, D. B., Kitchen, N. R., & Drummond, S. T. (2013). Modeling soil electrical conductivity–depth relationships with data from proximal and penetrating ECa sensors. *Geoderma, 199*, 12-21, doi:http://dx.doi.org/10.1016/j.geoderma.2012.10.006.

Sun, Y., Druecker, H., Hartung, E., Hueging, H., Cheng, Q., Zeng, Q., et al. (2011). Map-based investigation of soil physical conditions and crop yield using diverse sensor techniques. *Soil and Tillage Research, 112*(2), 149-158, doi:http://dx.doi.org/10.1016/j.still.2010.12.002.

Triantafilis, J., & Monteiro Santos, F. A. (2013). Electromagnetic conductivity imaging (EMCI) of soil using a DUALEM-421 and inversion modelling software (EM4Soil). *Geoderma, 211–212*, 28-38, doi:http://doi.org/10.1016/j.geoderma.2013.06.001.

Triantafilis, J., Roe, J. A. E., & Monteiro Santos, F. A. (2011). Detecting a leachate plume in an aeolian sand landscape using a DUALEM-421 induction probe to measure electrical conductivity followed by inversion modelling. *Soil Use and Management, 27*(3), 357-366, doi:10.1111/j.1475-2743.2011.00352.x.

Triantafilis, J., & Santos, F. A. M. (2009). 2-Dimensional soil and vadose-zone representation using an EM38 and EM34 and a laterally constrained inversion model. [Report]. *Australian Journal of Soil Research, 47*, 809+.

Triantafilis, J., & Santos, F. A. M. (2010). Resolving the spatial distribution of the true electrical conductivity with depth using EM38 and EM31 signal data and a laterally constrained inversion model. [Report]. *Australian Journal of Soil Research, 48*, 434+.

Triantafilis, J., Terhune Iv, C. H., & Monteiro Santos, F. A. (2013). An inversion approach to generate electromagnetic conductivity images from signal data. *Environmental Modelling & Software, 43*, 88-95, doi:http://dx.doi.org/10.1016/j.envsoft.2013.01.012.

Zhdanov, M. S. (2015). *Inverse theory and applications in geophysics* (Second ed., Vol. 36). Oxford: Elsevier.